Sodium-Ion-Conducting Hydrogel Material: Synthesis, Characterization and Conductivity Studies

Shashikant Yadav,[a] Dipendra Kumar Verma,[a] Rudramani Tiwari,[a] Devendra Kumar,[a] Km Parwati,[a] Rajshree Rai,[a] Pubali Adhikary,[b] and S. Krishnamoorthi*[a]

Herein we have reported single sodium ion conducting pseudo solid polymer electrolyte material, was synthesized successfully using sodium; 3,4,5,6-tetrahydroxyoxane-2-carboxylate (ALG) and sodium salt of poly (acrylic Acid): SPA in the water as solvent via solution cast technique. This pseudo-solid polymer material allows Na^+ cation transport inside the matrix. The FTIR technique confirmed the appreciable interaction between the sodium alginate and sodium polyacrylate polymer. This amorphous polymer material has good flexibility, tensile strength, and good elasticity which provides a better electrode-electrolyte interface. The material shows electrical conductivity in the range of 10^{-5} S/cm at room temperature and 10^{-4} S/cm at higher temperatures ($>40\,°C$). The material shows electrochemical stability of 2.26 V owing to a very good amount of current density with $\approx 97\%$ ionic transport number for the sodium ion. The material shows drift ionic velocity in the range of 10^{-4} m/s and ionic mobility in the order of 10^{-6} m²/Vs at room temperature. It shows the matrix ionic diffusivity constant in the order of 10^{-7} m²/s. It possesses low activation energy for ionic movement inside the matrix of 0.465 eV. The matrix shows the correlated type of hopping. An appreciable amount of capacitance is associated with the matrix with minute electrode contribution.

Introduction

Energy storage is a major challenge for the fast-developing world. The old-fashioned energy storage devices use liquid electrolytes due to outstanding wettability on the electrode surfaces and good conductivity.[1] Despite these advantages, liquid electrolyte-based energy storage devices have noticeable and unavoidable shortcomings viz; electrolyte leakage, portability, and wearability problems due to their large size, low ion selectivity, electrochemical instability, and potential risk.[2] Compared with liquid electrolytes, pseudo-solid state, and solid-state electrolytes[3] have the advantage of stabilized phase properties, higher thermal stability, longer device cycle life due to intrinsic slower reactivity,[4] and a physical barrier layer to separate negative and positive electrodes which avoids the leakage risk of electrolyte material and restrict the thermal runaway at higher temperature or shock.[5]

Lithium-ion-based electrolyte materials have frequently been used for a few decades but due to some critical drawbacks viz; flammable nature, narrow working temperature range, very limited natural abundance, and high cost associated with it, motivate researchers to think of an alternative to lithium-ion, in which sodium ion based solid polymer electrolyte (SPE) are found very promising one and nowadays intensively being used due to its low cost, high natural abundance, non-flammable, high safety and environmental sustainability hence sodium ion based SPEs have a high potential for the large scale energy storage.[6,7] Nowadays, hydrogel-based energy storage materials are very good to their liquid counterpart due to their chemical stability, softness, gel-like texture, flexibility, large electrochemical window, good thermal stability, high ionic conductivity, high electrode surface permeability, and efficiencies to attract and localize the ions due to the presence of trapped water as a solvent inside the hydrogel matrix. Despite of high dielectric constant of water and its excellent properties as an electrolyte, the water-based liquid electrolyte shows narrow electrochemical stability windows (ESW) up to 1.6 V and thermal stability in the range of $100\,°C$.[8] To overcome this atrocity water in salt approach is very promising to widen the ESW of water-based electrolyte systems. Here organic salt material plays an important role in widening ESW by minimizing the presence of interfacial water at the negative electrode surface and creating a uniform interphase that consist of an inner layer rich with inorganic metal ion and an organic outer layer. Such interphase minimizes the water reduction reaction at the electrode and enhances the ESW of the water-based system was reported up to 3.07 V[9,10] The thermal stability of water-based electrolyte systems is improved using polar organic salt material.[11] These organic materials trap the water molecule via hydrogen bonding and non-covalent interactions and retain the water molecule at higher temperatures. It is also reported that trapped water molecules in hydrogel for water in salt electrolytes are stable up to $140–150\,°C$[12] The blend hydrogel based on two or more polymers has flourishing interest these days. Blend-hydrogel based on the compatibilization of carbohydrate

[a] S. Yadav, D. Kumar Verma, R. Tiwari, D. Kumar, K. Parwati, R. Rai, Prof. S. Krishnamoorthi
Department of Chemistry, Centre of Advanced Study, Institute of Science, Banaras Hindu University, 221005 Varanasi, India
)
E-mail: skmoorthi@bhu.ac.in

[b] Dr. P. Adhikary
SATHI, NMR Lab, Central Discovery Centre, Institute of Science, Banaras Hindu University, 221005 Varanasi, India

ChemistrySelect

Research Article
doi.org/10.1002/slct.202302589

Chemistry Europe
European Chemical
Societies Publishing

and conducting compounds has a reckoning interest in the field of modern polymer technology due to the associated environmental benign and biodegradability of these materials.[13,14] The main difficulty associated with aqueous electrolyte-based hydrogel is solvent evaporation as well as oxygen evolution reaction (OER) and hydrogen evolution reaction (HER)[15,16] due to splitting of water which leads to atrocious results like safety issues, short device life cycle, and low coulombic efficiency. To overcome these shortcomings hydrogel material with hydrophilic functionality is the best alternative due to their associated inter as well as intra-hydrogen bonding capability which enhances the self-healing ability, flexibility, stretchability, etc.,[17] of the hydrogel material. Sodium alginate (ALG) is a naturally occurring polysaccharide having a large number of sodium ions associated with its functional group. It is a biopolymer extracted from seaweed.[18,19] Alginate has wide application potential in our everyday life mainly in the food, textile industries, medical and pharmaceutical industries. Alginate has very good gelation properties due to which it can be used in combination or by itself with other polymers and is hence very suitable in the synthesis of hydrogel material with tunable mechanical properties.[20,21] The presence of the carboxylate group enables a large number of hydrogen bonding capabilities[22] in alginates and is linked to its ability to retain water, viscosifying and stabilizing properties, etc. Due to this, it has good self-healing[23] properties which makes it a promising material for tissue engineering.[24] The presence of an evenly distributed large number of hydroxyl and carboxylic groups in the alginate backbone enhances its interaction properties as well as cross-linking ability that provides ion transport with supported ion hopping between the adjacent sites. Liu et al. suggested that alginate can interact non-covalently with other multivalent cations which leads to higher capacity retention and longer cycle life for electrode. Alginate enhances the coulombic efficiency and charge storage capacity for sodium-ion batteries as suggested by Ling et al.[25,26] Sodium polyacrylate (SPA) is an anionic polymer with the carboxylic group on the polymer backbone and it is a superabsorbent waterlock polymer compound.[27] SPA has very good blend-forming capacity, thermal stability, electrochemical performance, composite and film-forming ability with metal ions due to these associated properties it is a good promising material in the fields of drug delivery, food industries, soil improvement,[28] plant growth[29] and energy storage devices, fuel cell, etc. As SPA contains a good concentration of polar carboxylate groups it has very good film-forming and waterlock properties and is also a rich source of sodium ions. Moreover, SPA has good adhesion ability which makes it a promising material for electrode surface interaction. SPA can act as a good crosslinking agent that interacts more strongly via hydrogen and ionic bonding with materials. This property led to improved cell performance and capacity retention by forming stable solid electrolyte interphase.[30,31] The SPA network interacts with water via H-bonding and minimizes the hydrogen evolution reaction thus widening the ESW and enhancing the thermal stability of the polymer matrix system. Due to all these above-discussed properties, ALG and SPA will become the best combination for

energy storage hydrogel polymeric material without using an added cross-linking agent as here SPA itself acts as a cross-linker.

In this work, we have prepared ALG and SPA-based single ion conducting hydrogel electrolyte material (ALG-SPA) made up of 60% (w/w) SPA and 40% (w/w) ALG synthesized by solution casting technique using water as solvent. The well-prepared hydrogel film was characterized by various methods such as structural, vibrational, morphological, and ionic conductivity studies, dielectric properties, cyclic voltammetry, and transference number analysis. The temperature-dependent study of hydrogel material was also performed between 20 °C to 80 °C to see the change in electrical and dielectric behavior.

Experimental

Preparation of Sodium alginate- Sodium polyacrylate (ALG-SPA) electrolyte

The preparation of ALG-SPA polymer hydrogel electrolyte was made by dissolving 40% (w/w) of sodium alginate into 60%, (w/w) SPA respectively. This solution was poured into a polypropylene petri dish. The weight of the solution-filled petri dish was recorded at this stage. The material was then subjected to a 48 h drying process in an oven at 50 °C under controlled conditions, followed by a re-weighing of the petri dish. We got ALG-SPA material with 15% (w/w) water content inside the matrix. (Scheme 1).

Result and Discussion

The hydrogel polymeric material ALG-SPA was successfully synthesized via the solution cast technique using water as solvent. The solvent molecules allow the homogeneous mixture of sodium alginate and sodium polyacrylate due to intermolecular attraction between ALG-SPA as shown in (Scheme 1). When the solution was allowed to dry some solvent molecules were trapped inside it and we got a pseudo-solid hydrogel polymer material with an immobilized anionic component with a single cationic component inside the polymer matrix that contributes towards conductivity. The solvent molecule weakly interacted with both ALG and SPA via hydrogen bonding and provided stretchability and non-flammable characteristics to the hydrogel matrix. Since the preparation of ALG-SPA hydrogel material was performed using green solvent without heating at room temperature and alginate is an environmentally friendly, biocompatible natural polymer material, we can say this was the greener approach which provides the low-cost, non-hazardous, and environmentally benign conducting hydrogel material.

IR spectroscopy

The synthesized polymer was investigated using the infrared spectroscopy technique as shown in Figure 1A. A characteristic absorption stretching vibration in the range of 3200–3600 cm^{-1} due to the stretching vibration band of —OH group in ALG

ChemistrySelect

Research Article
doi.org/10.1002/slct.202302589

Chemistry Europe
European Chemical
Societies Publishing
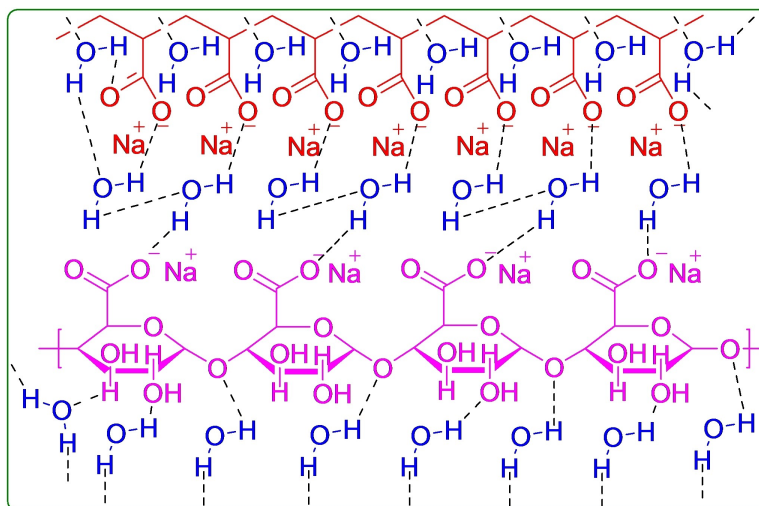
Scheme 1. Plausible interaction scheme for ALG-SPA polymer matrix.
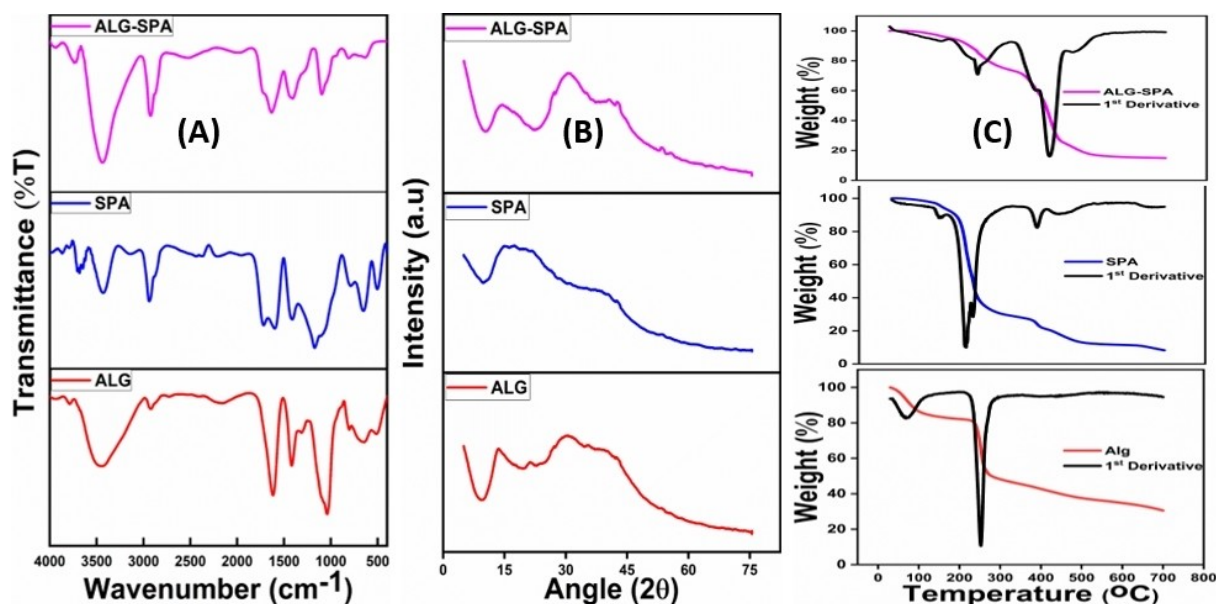
Figure 1. (**A**) IR Spectrum of ALG, SPA, and ALG-SPA (**B**) showing XRD for ALG, SPA, and ALG-SPA (**C**) TGA plot for ALG, SPA and ALG-SPA polymer matrix

which shifted to 3200–3400 cm^{-1} due to hydrogen bonding in the blend. A peak near 2928 cm^{-1} in the ALG-SPA blend is observed due to C−H stretching vibration of SPA which is at 2920 cm^{-1} in SPA polymer. The bending vibration near 2540 cm^{-1} in ALG-SPA is due to O−H of water interacting with C=O of SPA inside the blend. The band at 1605 cm^{-1} and 1420 cm^{-1} were attributed to asymmetric and symmetric vibration of the COO$^-$ group respectively[32] which is shifted to 1620 cm^{-1} and 1430 cm^{-1} respectively in the blend. The peak at 1730 cm^{-1} is attributed to C=O stretching vibration in SPA which shifts to 1738 cm^{-1} in the ALG-SPA blend matrix. The shoulder at 1090 cm^{-1} in ALG is attributed to C−O stretching vibration which shifts to 1105 cm^{-1} in the ALG-SPA blend.[33–35]

XRD

The X-ray diffraction pattern of neat SPA, ALG, and the ALG-SPA polymer matrix is shown in Figure 1B. There is an appreciable change observed in the SPA and ALG after the formation of the ALG-SPA matrix. There are broad peaks near 19° and 40° theta values showing low crystallinity of the SPA polymer. While ALG shows a large number of peaks such as 13.4°, 17.4°, 21.5°, 26.5°, and between 30.7 to 42.5° indicating a more crystalline nature than SPA. While the ALG-SPA polymer matrix shows peaks at 14.7°, 27°, 30.3°, 42.7°, and new diffraction peaks at 54.2°, and 56.04°. Since alginate and polyacrylate both are polymeric materials with hydrocarbon backbone (low Z) they show amorphous broad peaks in X-ray. Because of hydrogen bonding, the good compatibility between alginate and poly-

acrylate exists and is attributed to a decrease in crystallinity of the hydrogel material resulting in a broad amorphous peak which shows the semicrystalline nature and different packing arrangement of the materia.[36]

TGA

The synthesized polymer was analyzed thermogravimetrically to know the thermal stability as shown in Figure 1C. The ALG polymer shows two major weight losses. The first weight loss of ~ 11% up to 120 °C was attributed to the removal of moisture from the ALG polymer. The second weight loss of 34% in the temperature range of 190 °C to 260 °C was due to the degradation of the sample which led to the loss of CO_2 gas from the polysaccharide backbone and degradation above 290 °C was due to pyrolysis of the polymer backbone.[37] The SPA polymer shows a three-step degradation pattern. The first weight loss of 9% up to 190 °C was due to the loss of absorbed water molecules in the SPA polymer. The second weight loss of 67% in the temperature range of 190 °C to 300 °C was attributed to the removal of CO_2 gas from the SPA matrix. The third weight loss >300 °C was due to the degradation of the polymeric chain. The ALG-SPA hydrogel matrix shows four-step degradation patterns. The first weight loss of 6% up to 130 °C was observed due to the loss of moisture from the surface of the polymer matrix. The second weight loss of 15% in the range of 130 °C to 200 °C was due to the removal of trapped water inside the matrix. The third major weight loss of 46% in

the temperature range of 200 °C to 320 °C was due to the loss of CO_2 gas from the matrix, and degradation above 320 °C was due to the pyrolysis of the polymer matrix.[38] Thus, the synthesized material is thermally stable and suitable for applications up to 200 °C.

Electrochemical analysis

Electrochemical analysis of prepared electrolyte material was performed by using two electrode systems where standard (SE) and counter (CE)) were clubbed together and the sample was sandwiched between two stainless steel blocking electrodes i.e. SS|ALG-SPA|SS cell setup which works as a working electrode. The prepared sample has a thickness of ~ 500 μm and the surface area of the working electrode was 0.5 cm². The Cyclic Voltammetry (CV) data is recorded in the voltage range of -0.5 V to 3 V and a scan rate of 10 mVs^{-1} as shown in Figure 2A. The plot shows there is no oxidation-reduction peak in the electrochemical stability window region. The voltammogram substantiates the large amount of charge density associated due to capacitive behavior of the polymer material. The linear sweep voltammetry (LSV) analysis was performed to study the electrochemical stability window (ESW) of the polymer material. This measurement was performed in the voltage range of 0 V to $+4$ V and a scan rate of 10 mVs^{-1} at room temperature as shown in Figure 2B. It shows a plateau current region up to 2.26 V which confirms the stability of material without oxidation. Above 2.26 V there is a sharp
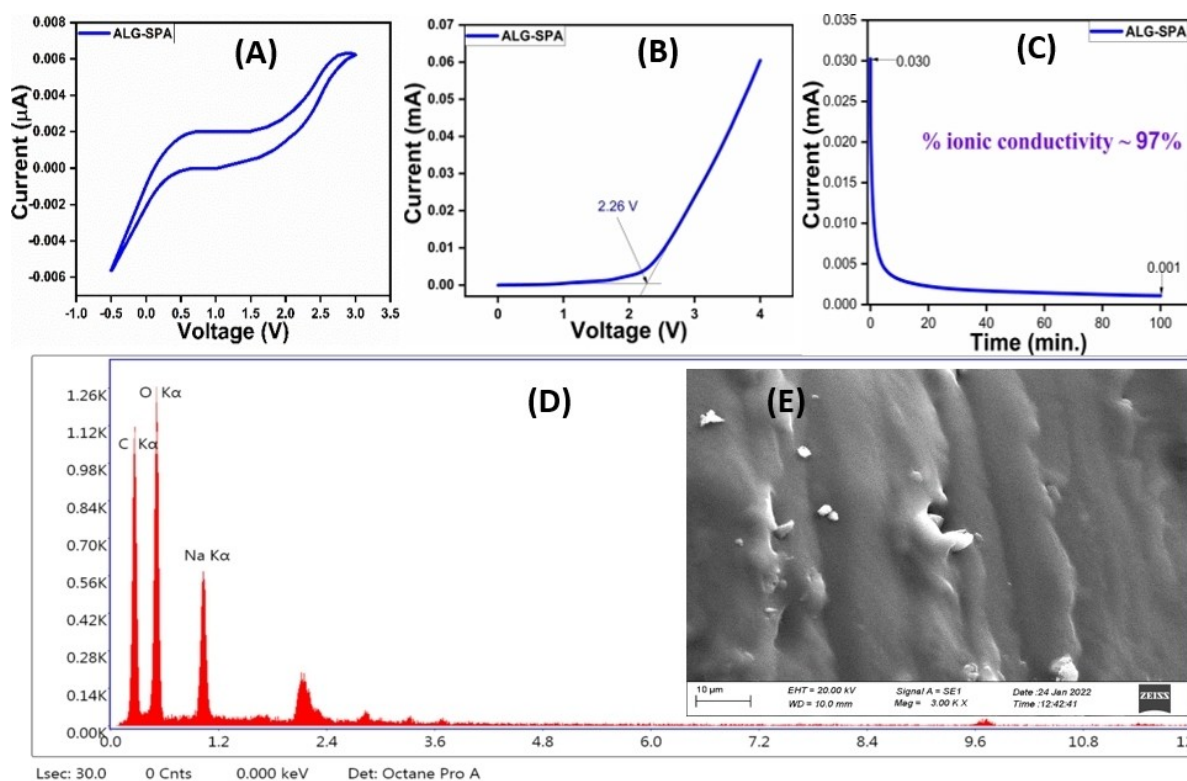
Figure 2. For ALG-SPA polymer matrix (**A**) Cyclic voltammetry curve (**B**) LSV analysis curve (**C**) chronoamperometric plot (**D**) EDS spectrum (**E**) SEM analysis image.

ChemistrySelect

Research Article
doi.org/10.1002/slct.202302589

Chemistry Europe
European Chemical
Societies Publishing

increase in current observed which is the result of the oxidation of constituents of matrix. The ESW value was measured by drawing tangents on the LSV plot, one parallel to the Plateau region and another on the curve after the plateau region. The intersection point of these two tangents corresponds to the ESW value of 2.26 V.[39] It is reported in the literature that free water molecules get oxidized at 1.23 V due to oxidation of the oxygen atom of water but when a water molecule interacts with any other molecule, it leads to the suppression of water decomposition reactions and electrochemical stability widens due to different chemical environment.[40] This widened ESW value confirms the applicability of prepared material in device fabrication and other energy storage uses.

Chronoamperometric measurement

Ionic transference number (ITN) was analyzed using chronoamperometry analysis. It is defined as the ability to carry the fraction of total current by each ion inside the polymer matrix. It is the important parameter that measures the movement of ions inside the polymer matrix under the influence of external potential which in turn affects the contribution of each ion to total conduction i.e.; conductivity inside the polymer matrix along with stability, cycle life, and efficiency of energy storage devices. Here Wagner's DC polarization method was employed to perform the ITN and nature of charge carriers i.e., electronic or ionic. The polarization curve (Figure 2C) shows a rapid decrease in the initial current (I_i) value from its initial value and a continuous drop up to 6000 seconds which gives the final current value (I_f). The ITN was calculated using the following equation (1):

$$I_{ion} = (I_i - I_f)/I_i \qquad (1)$$

The rapid decrease in the initial current as shown in (Figure 2C) is due to the depletion of ionic species in the polymer matrix and attaining constant in the fully depleted region. For the ALG-SPA polymer matrix, ITN was found to be ≈97%. This high value of ITN will be very helpful in order to get high power density, faster charge and discharge rates, and also minimize the risk of ion accumulation at electrodes in energy storage devices.[41]

SEM-EDAX analysis

A scanning electron microscope (Zeiss model EVO 18 Research) at 20 kV was used for the analysis of the surface morphology and elemental composition of prepared ALG-SPA. The elemental composition and distribution were analyzed by selecting a specific area of the hydrogel matrix at different positions. The electron beam from the scanning microscope bombarded the sample, and the ground state electrons were excited to a higher energy level. These electrons return to the ground state by radiatively emitting X-rays with characteristic information about the element. In this way, the composition of all elements

present within the sample is quantified. The EDAX plot Figure 2D shows uniform distribution with the presence of carbon, oxygen, and sodium elements in the polymer matrix with percentage compositions of 53%, 35%, and 12%, respectively. SEM micrograph is shown in Figure 2E at 3.00 KX magnification with micro-scale resolution. Since alginate-based hydrogels are typically nanoporous as reported by Singh V et al.[42] A very compact, smooth, and wavy layered texture was obtained due to the strong interaction between sodium alginate backbone with trapped water and sodium polyacrylate which leads to the uniform homogeneous aggregated matrix that may suppress the pores inside the matrix. The detailed selected area EDS report is attached in supporting data.

Electrical Conductivity

The electrical conductivity and dielectric study of the ALG-SPA polymer material were performed using the electrochemical impedance spectroscopic (EIS) technique. A typical Nyquist plot which is plotted between the real (Z') and imaginary (iZ'') part of electrical impedance as shown in Figure 3A represents the ionic conductivity of the polymeric material at room temperature as well as at higher temperatures. The Nyquist plot follows the complex impedance relation as shown in equation (2):

$$Z^* = Z' - iZ'' \qquad (2)$$

Where Z^* represents the complex impedance. The semicircular part of the Nyquist plot provides the bulk resistance (R_b) which was an interface of the imaginary part on the real part of the impedance at the lower frequency side and from that the DC conductivity (σ_{dc}) or the bulk conductivity of the polymeric material calculated using the equation (3):[43]

$$\sigma_{bulk} = (1/R_b)\,(l/A) \qquad (3)$$

Where A and l are the cross-sectional areas of the polymeric film electrode surface and thickness (cm) of the film respectively.

The conductivity of the ALG-SPA polymer matrix at room temperature was found in the range of 10^{-5} S/cm and it increases with temperature at 80°C the conductivity was observed in the order of 10^{-4} S/cm. The amorphous nature of the polymer material assisted in better conduction of ions inside the polymer matrix and the matrix got tranquil at a higher temperature which allowed the smooth movement of ions inside the matrix which was the key reason for the gradual increase in conductivity with temperature. The idea about the flow of charge and ion transport behavior inside the matrix was confirmed by the AC conductivity study. The bulk AC conductivity as a function of frequency is shown in Figure 3B. The AC conductivity can be analyzed and fitted using Jonscher's power law (JPL) shown in equation (4):

ChemistrySelect

Research Article
doi.org/10.1002/slct.202302589

Chemistry Europe
European Chemical
Societies Publishing
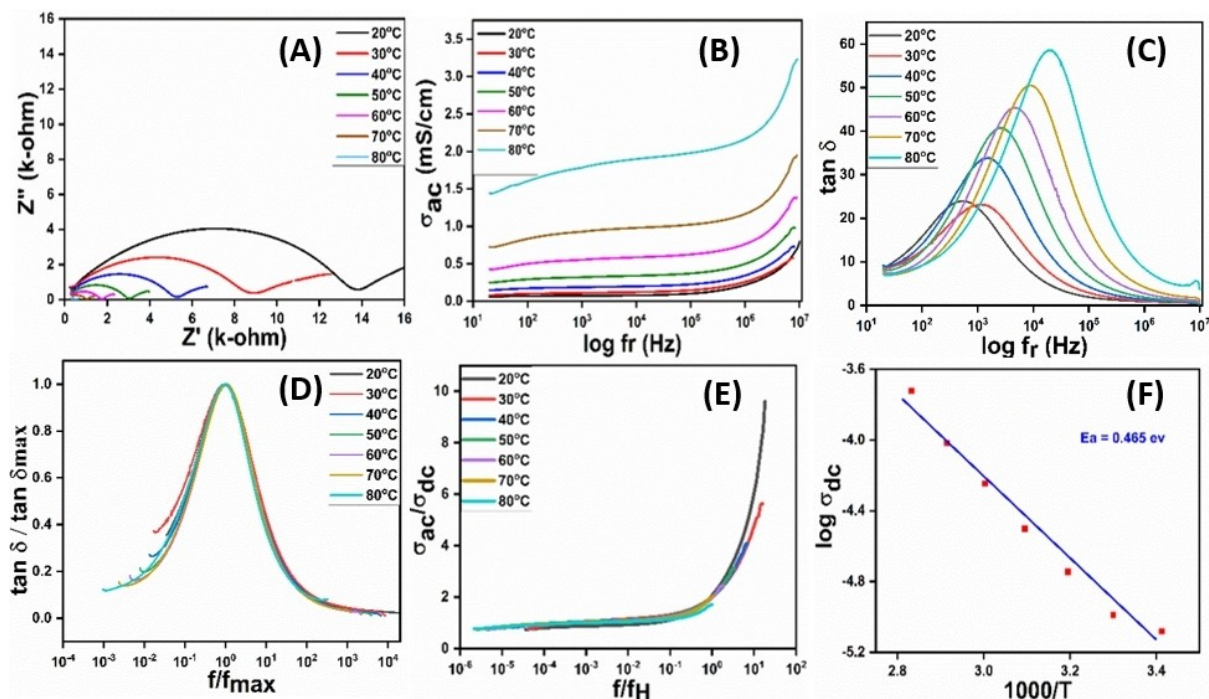
Figure 3. For ALG-SPA polymer matrix **(A)** Cole-Cole plot at different temperatures **(B)** AC conductivity plot at different temperatures **(C)** Loss tangent plot at different temperatures **(D)** Scaled loss tangent master curve plot at different temperatures **(E)** Scaled AC conductivity master curve at different temperature **(F)** log σ_{dc} vs 1000/T plot showing Arrhenius type behavior.

$$\sigma_{ac} = \sigma_{dc} + A\omega^n \tag{4}$$

where σ_{dc} represents the direct conductivity of the polymer material, A is constant represents the dispersion parameter and ω represents the angular frequency, n represents the value of power exponent. The value of the power exponent (n) for ALG-SPA polymer shows n < 1 which represents the correlated type hopping of ions inside the polymer matrix. In Figure 3B we observe a plateau in mid mid-frequency region representing the frequency-independent bulk DC conductivity (σ_{dc}) of the polymer matrix. The value of σ_{dc}, A, n, and R^2 the fitting parameter for plot fitting at different temperatures is provided in table S1. The movement of ions inside the polymer matrix increases with an increase in temperature and shows the Arrhenius-type thermally activated process as shown by equation (5):

$$\sigma_T = \sigma_o\ exp^{-Ea/kT} \tag{5}$$

Where σ_o is the pre-exponential factor, k is the Boltzmann constant and T is the temperature in (K). E_a is the activation energy. Figure 3F shows the plot between log σ_{dc} vs. 1000/T of the polymer matrix and exhibits the linear variation from that it is clear that log σ_{dc} is progressively increased with temperature and so the amorphousness of the polymer matrix which allows the smooth movement of ions inside the matrix and the activation energy for the ionic movement was found to be 0.465 eV which is quite low for the ionic conduction.

The dielectric relaxation study shown in plot (Figure 3C) which is plotted between the dielectric loss tangent (tan δ) vs.

frequency, in which dielectric loss tangent (tan δ) is represented by the equation (6) as following:

$$tan\ \delta = \varepsilon''/\varepsilon' \tag{6}$$

Where ε' is the real part and ε'' is the imaginary part of the complex dielectric permittivity (ε^*). This study revealed the effect of temperature on the polymer matrix polarization and relaxation which are equally responsible for the conduction of ions inside the polymer matrix. It is clearly shown in Figure 3C that the relaxation band increases with a rise in temperature up to a maximum value and then decreases with increasing frequency which is basically due to amplification in the flexibility of the polymer chain which is responsible for higher ionic conduction. Figure 3E represents the scaled AC conductivity curve plotted between σ_{ac}/σ_{dc} vs. f/f_H. This scaling was performed into a single master curve for all temperatures. The hopping frequency f_H obtained from the AC conductivity plot which was the frequency parallel to the onset of conductivity diffusion is given by the power law relation[44] as shown in the equation (7):

$$f_H = (\sigma_{dc}/A)^{1/n} \tag{7}$$

Since we got an overlapped single conductivity curve for all temperatures, this specifies the temperature-independent matrix relaxation process under ionic conduction. The observation about change in relaxation time with varying electric field and temperature was reckoned from scaled loss tangent spectra

ChemistrySelect

Research Article
doi.org/10.1002/slct.202302589

Chemistry Europe
European Chemical
Societies Publishing

(tan δ) and was described by Kohlrauch Williams-Watt's law[45] as shown in equation (8):

$$f(t) = exp\,(-t/\tau)^{\beta} \tag{8}$$

Where β is the Kohlrauch exponent. The scaled loss tangent plot at different temperatures (Figure 3D) shows a merged single master curve which indicates the time-independent relaxation process under ionic conduction. The polymer matrix does not follow the Debye-type relaxation mechanism and this was confirmed by the Kohlrauch exponent (β) shows $0<\beta<1$ calculated from the master curve.

The dielectric formalism gives the idea about the ion conduction inside the polymer matrix. Figure 4(A–B) shows the variation of dielectric permittivity with frequency, where ε' which is the real part of the dielectric permittivity represents the charge storage capacity of the polymer matrix and ε'' which is the imaginary part of the dielectric tells about the energy loss due to the movement of the charge carriers inside the polymer matrix. Figure 4(A–B) clearly shows the high value of permittivity at the lower frequency region was attributed due to the formation of a double layer because of the accumulation of ions at the electrode-electrolyte interface however a constant value obtained at the high-frequency region because the ions fail to follow the field.[46]

In Figure 4B we observed a relaxation peak in the mid-frequency region which appears because of the fast periodic reversal of the electric field initially on the high-frequency side due to small pores present on the surface of the matrix and then slow periodic reversal because of the layered structure

inside the polymer matrix. The variation of dielectric modulus with frequency gives the idea about the electrode-electrolyte interface. The variation of the real part M' and imaginary part M'' of complex dielectric modulus M^* as a function of frequency for ALG-SPA polymer matrix is shown in Figure 4(D–E). The longer tails observed in the lower frequency region were due to huge capacitance allied with polymer matrix and negligible electrode polarization effect which rejected any false contribution to the dielectric constant, and the values of M' and M'' increases at higher frequency were due to the bulk effect of resistance.[47,48]

The bulk ionic conductivity (σ_{dc}) depends on the transport factors such as concentration of charge carriers (N), diffusion coefficient (D), and mobility (μ).[49] The σ_{dc} depends on these parameters as shown in the equation (9):

$$\sigma_{dc} = N\mu q \tag{9}$$

Where q is the elementary charge on the ion.

Whereas the relation betweeen concentration of charge carriers (N) and diffusion coefficient shown by following equation (10):

$$N = (\sigma_{dc}\,k_b\,T)/Dq^2 \tag{10}$$

The ionic diffusivity coefficient (D) is a very important parameter that measures the efficacy of rapid diffusion of ions inside the polymer matrix under the influence of an external
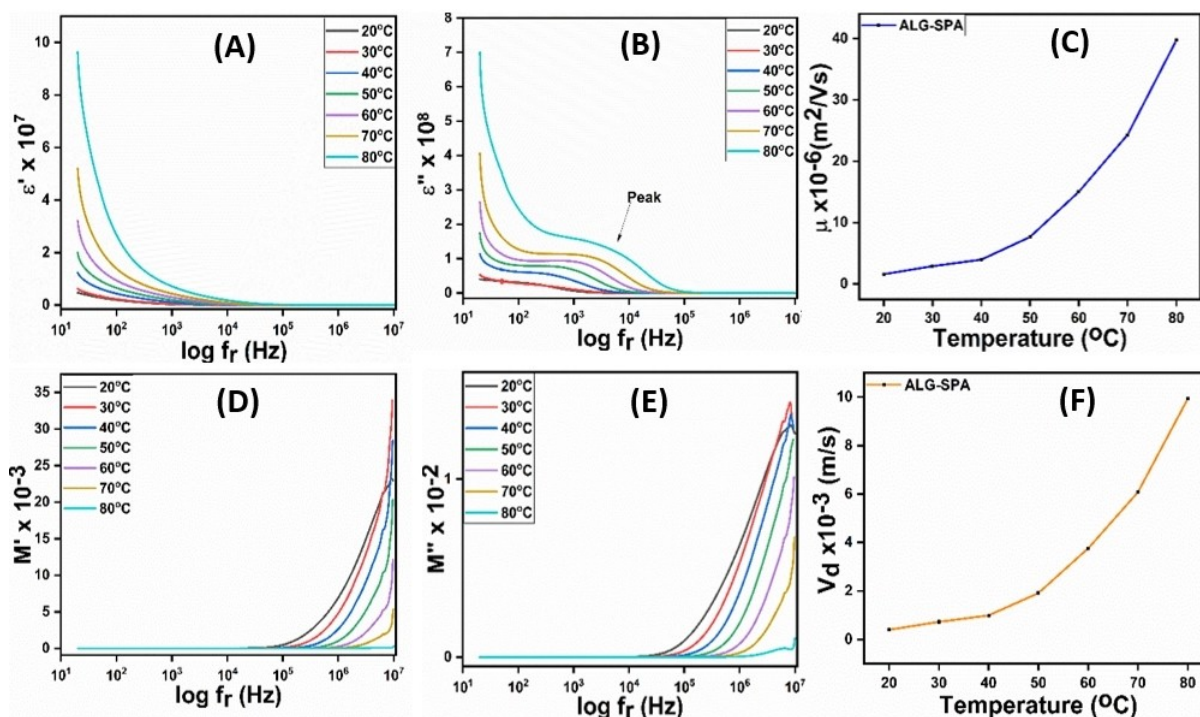
Figure 4. For ALG-SPA polymer matrix **(A)** Showing real part of dielectric permittivity at different temperatures **(B)** Imaginary part of dielectric permittivity at different temperatures **(C)** Ionic mobility plot **(D)** Real part of electric modulus at varying temperature **(E)** Imaginary part of electric modulus at varying temperature **(F)** Drift velocity curve.

ChemistrySelect

Research Article
doi.org/10.1002/slct.202302589

Chemistry Europe
European Chemical
Societies Publishing

electric field. Ionic diffusivity is calculated using the equation (11):[50]

$$D = 2\, f_{max}\, l^2/32\, (tan\, \delta_{max})^3 \tag{11}$$

Moreover, the following equation (12) shows the dependency of the ionic mobility (μ) inside the polymer matrix on the total number density of carrier ions:

$$\mu = \sigma_{dc}/Nq \tag{12}$$

Figure 4(C) & (F) represent the plot of ionic mobility and drift ionic velocity (V_d) respectively. The ionic mobility (μ) is related to the ionic conductivity and concentration of ions by the Nernst-Einstein[51–53] equation (13):

$$\sigma = F \sum (z^2\, c\, \mu) \tag{13}$$

Where σ is the ionic conductivity, F is Faraday's constant, z is the charge on the ion, c is the concentration of the ion. It is clear from Figure 4(C) that the value of ionic mobility increases with the rise in temperature hence the bulk DC conductivity. The drift ionic velocity is the important factor that provides the gist of how fast an ion moves inside the polymer matrix. Figure 4(F) shows a camber nature of increment with temperature and this was due to the diverse speed of the ions which results from the small amount of collision of ions with the polymer chain of the matrix. In equation (14) the Arrhenius relation shows the temperature dependency of drift velocity:

$$V_d = V_{do} e^{-Ea/KT} \tag{14}$$

Again, the drift ionic velocity is also related to the ionic conductivity as equation (15):

$$\sigma = z\, V_d\, N \tag{15}$$

Where z is the ionic charge and N is the number density of the ions inside the matrix. It is clear from the plot that a higher value of drift velocity is very helpful in order to get high efficiency of energy storage devices.

The values of C_b, ε_b N, D, μ, and V_d at varying temperatures are given in Table S1.

Conclusions

The ALG-SPA based hydrogel polymer matrix was successfully synthesized via the solution cast technique. The interactions between the ALG and SPA were confirmed using FTIR spectroscopy. The amorphous nature of the ALG-SPA polymer matrix was verified using the XRD technique. Synthesized polymer matrix showed thermal stability up to 200 °C confirmed by TGA analysis due to which this material is fit for applicable over a wide temperature range. A compact, smooth, and wavy surface morphology was confirmed using SEM analysis. The EIS technique confirmed the semiconducting nature of polymer matrix with good bulk DC conductivity in the range of 10^{-5} S/cm at room temperature and 10^{-4} S/cm at higher temperature (>40 °C) and shows a correlated type of hopping with n < 1. The material shows an electrochemical stability window of 2.26 V with a quite appreciable current density associated with it. The ionic transference number $\approx 97\%$ shows an appreciable number of ions associated with the polymer matrix and conduction is ionic. The material follows the Arrhenius type of conduction mechanism and the energy of activation for ion movement inside the matrix was 0.465 eV. The time-temperature independence of ionic conduction was verified by a scaled AC plot. The loss tangent plot confirms the low value of matrix relaxation at lower frequency region which increases with the rise in frequency. The dielectric permittivity analysis confirms a large amount of capacitance associated with the material and the negligible electrode contribution at the electrode-electrolyte interface was verified from the electric modulus study. The material shows an increment in drift velocity and ionic mobility with temperature. The value of D, N, μ, and V_d for 40% ALG-SPA was 4.07×10^{-8} m²/s, 2.75×10^{19} m⁻³, 1.29×10^{-7} m²/Vs, and 4.03×10^{-4} m/s respectively. Since the synthesized 40% ALG-SPA polymer material has very good thermal stability, environmental sustainability, electrical semi-conductivity, charge storage capacity, and a high value of ionic transference number makes this material is the best candidate for energy storage devices.

Supporting Information Summary

Materials, synthetic procedures, sample characterization method, complete EDS report, and Table S1 are provided as supporting information.

Conflict of Interests

The authors declare no conflict of interest.

Data Availability Statement

The data that support the findings of this study are available from the corresponding author upon reasonable request.

[1] Selvaraj, Tinesha, V. Perumal, S. F. Khor, L. S. Anthony, S. C. B. Gopinath, N. M. Mohamed, *Mater. Res. Bull.* **2020**, *126*, 110839.

[2] S. Shenbagavalli, M. Muthuvinayagam, M. S. Revathy, *Ionics* **2023**, *29*, 211-231.

[3] S. Yadav, R. Tiwari, D. K. Verma, D. Kumar, P. Adhikary, S. Krishnamoorthi, *Polym. Eng. Sci.* **2023**, *63*, 584–592.

[4] -Maia, B. Arouca, N. Magalhães, E. Cunha, M. H. Braga, M. Raquel, Santos, N. Correia, *Polymer* **2022**, *14*, 403.

[5] P. Yao, H. Yu, Z. Ding, Y. Liu, J. Lu, M. L. J. Wu, X. Liu, *Front. Chem.* **2019**, *7*, 522.

[6] -Lukasiewicz, Marcin, A. Ptaszek, L. Koziel, B. Achremowicz, M. Grzesik, *Polym. Bull.* **2007**, *58*, 281–288.

[7] -Pyarasani, D. Radha, T. Jayaramudu, A. John, *J. Mater. Sci.* **2019**, *54*, 974–996.

[8] M. Jakub, E. Frackowiak, K. Fic, *J. Power Sources* **2019**, *414*, 183–191.

[9] Kuhnel, R. Simon, D. Reber, C. Battaglia, *J. Electrochem. Soc.* **2020**, *167*, 070544.

[10] R. Tiwari, D. K. Verma, D. Kumar, S. Yadav, K. Kumar, P. Adhikary, S. Krishnamoorthi, *Energy Fuels* **2022**, *36*, 6459–6467.

[11] G. Przemyslaw, A. Slesinski, K. Fic, J. Menzel, *J. Mater. Chem. A* **2021**, *9*, 8644–8654.

[12] R. Tiwari, D. K. Verma, D. Kumar, S. Yadav, K. Kumar, S. Krishnamoorthl, *Mater. Chem. Front.* **2021**, *5*, 5857–5866.

[13] S. Yiming, X. Ji, *Chem. Rev.* **2021**, *121*, 6654–6695.

[14] V. Zalm, M. Joshua, J. Quintal, S. A. Hira, S. Chen, A. Chen, *Electrochim. Acta* **2023**, *439*, 141715.

[15] -T. Liu, C. Jiao, X. Peng, Y. N. Chen, Y. Chen, C. He, R. Liu, H. Wang, *J. Mater. Chem. B* **2021**, *6*, 8105–8114.

[16] E. Su, M. Yurtsever, O. Okay, *Macromolecules* **2019**, *52*, 3257–3267.

[17] Q. Zhang, C. Liao, T. Zhai, H. Li, *Electrochim. Acta* **2016**, *196*, 470–478.

[18] S. H. Rashedy, S. M. A. E. H. Mohamed, M. A. Dar, J. Cotas, L. Pereira, *Appl. Sci.* **2021**, *11*, 6290.

[19] Abraham, Adiam, B. Afewerki, B. Tsegay, H. Ghebremedhin, B. Teklehaimanot, K. S. Reddy, *Int. J. Mar. Biol. Res.* **2018**, *3*, 1–8.

[20] L. Paola, *Mar. Drugs* **2010**, *8*, 2435–2465.

[21] H. Hadas, S. Srebnik, *Biomacromolecules* **2016**, *17*, 2160–2167.

[22] -I. Donati, A. Yrr, Mørch, B. L. Strand, G. Skjåk-Bræk, S. Paoletti *J. Phys. Chem. B* **2009**, *113*, 12916–12922.

[23] B. Francesca, F. D. Giorgio, F. Soavi, C. Arbizzani, *J. Electrochem. Soc.* **2016**, *164*, A6171.

[24] W. Jiang, G. Zhou, C. Wang, Y. Xue, C. Niu, *Constr. Build. Mater.* **2021**, *271*, 121541.

[25] S. Olav, G. Skja, *Trends Biotechnol.* **1990**, *8*, 71–78.

[26] K. Igor, B. Zdyrko, A. Magasinski, B. Hertzberg, Z. M. Ruslan, B. igor, Luzinoy, G. Yushin, *Science* **2011**, *334*, 75–79.

[27] L. Liming, Y. Bai, Z. Wang, Q. Ni, G. Chen, Z. Zhou, C. Wu, *ACS Appl. Mater. Interfaces* **2018**, *10*, 5560–5568.

[28] A. Georgios, A. Karakassides, M. Baikousi, C. Gioti, D. Moschovas, A. Avgeropoulos, B. Athanasios, A. P. Bourlinos, C. E. Douvalis, Salmas, M. A. Karakassides, *C* **2021**, *7*, 69.

[29] N. Özbakan, E. Burak, in *Proceedings of the 7th World Congress on Civil, Structural, and Environmental Engineering, Lisbon, Portugal-April 10–12*, **2022**.

[30] S. H. Hong, S. Y. Ham, J. S. Kim, I. S. Kim, E. Y. Lee, *Int. Biodeterior. Biodegrad.* **2016**, *113*, 297–303.

[31] Maitra, Jaya, V. K. Shukla, *Am. J. Polym. Sci.* **2014**, *4*, 25–31.

[32] S. Wenshuo, J. Zhu, Y. Liu, L. Kang, S. liu, B. Huang, J. Song, *ACS Appl. Mater. Interfaces* **2021**, *13*, 24756–24764.

[33] C. R. Badita, D. Aranghel, C. Burducea, P. Mereuta, *Rom. J. Phys.* **2020**, *65*, 1–8.

[34] S. Amarjargal, V. Kasparkova, T. Sedlacek, Petr Sáha, *J. Mech. Behav. Mater.* **2013**, *18*, 152–166.

[35] U. Koichi, S. Kikuchi, F. Mikami, Y. Kadoma, N. Kumagi, *J. Power Sources* **2007**, *173*, 518–521.

[36] C. Mingyu, J. Deng, F. Yang, Y. Gong, N. Zhao, X. Zhang, *Biomaterials* **2003**, *24*, 2871–2880.

[37] S. Ahmed, M. M. Sanagi, A. A. Naim, K. J. A. Karim, W. A. W. Ibrahim, U. Abdulganiyu, *Polym. Bull.* **2016**, *73*, 519–537.

[38] H. Daemiand, M. Barikani, *Sci. Iran.* **2012**, *19*, 2023–2028.

[39] S. Monisha, T. Mathavan, S. Selvasekarapandian, A. M. F. Benial, M. P. Latha, *Ionics* **2017**, *23*, 2697–2706.

[40] H. Yongxin, L. Zho, L. Li, M. Xie, F. Wu, R. Chen, *Adv. Mater.* **2019**, *31*, 1808393.

[41] D. K. Verma, R. Tiwari, D. Kumar, S. Yadav, K. Parwati, P. Adhikary, S. Krishnamoorthi, *J. mater. Sci. Eng. B* **2023**, *297*, 116.

[42] V. Singh, A. Singh, *Alginates: Versatile Polymers in Biomedical Applications and Therapeutics*, CRC Press, Boca Raton Florida **2019**, 159–170.

[43] P. Georén, G. Lindbergh, *Electrochim. Acta* **2001**, *47*, 577–587.

[44] S. Lanfredi, A. C. M. Rodrigues, *J. Appl. Phys.* **1999**, *86*, 2215–2219.

[45] D. P. Almond, A. R. West, *Solid State Ionics* **1983**, *9*, 277–282.

[46] H. K. Patel, S. W. Martin, *Phys. Rev. B* **1992**, *45*, 10292.

[47] D. J. Ojur, A. A. Adam, M. K. M. Ali, H. Soleimani, M. F. B. A. Shukur, K. H. Ibnaouf, O. Aldaghri, *Membranes* **2022**, *12*, 706.

[48] S. Ramesh, A. K. Arof, *J. mater. Sci. Eng. B* **2001**, *85*, 11–15.

[49] M. Hema, S. Selvasekarapandian, A. Sakunthala, D. Arunkumar, H. Nithya, *Phys. B* **2008**, *403*, 2740–2747.

[50] A. Abdukarimov, I. S. M. Noor, O. Mamatkarimov, A. K. M. Arof, *High Perform. Polym.* **2022**, *34*, 232–241.

[51] N, Srivastava, M. Kumar, *J. Solid State Electrochem.* **2016**, *20*, 1421–1428.

[52] M. C. Pang, M. Monica, H. Wang, G. Offer, *Phys. Chem. Chem. Phys.* **2021**, *23*, 27159–27170.

[53] D. K. Verma, R. Tiwari, D. Kumar, S. Yadav, P. Adhikary, S. Krishnamoorthi, *ChemistrySelect* **2023**, *8*, e202302287.